New Phytologist Supporting Information

The auxin efflux carrier PIN1a regulates vascular patterning in cereal roots

Riccardo Fusi[1,2], Sara Giulia Milner[3], Serena Rosignoli[3], Riccardo Bovina[3], Cristovão De Jesus Vieira Teixeira[1,4], Haoyu Lou[1,5,6], Brian S. Atkinson[1], Aditi N. Borkar[7], Larry M. York[1,8], Dylan H. Jones[1], Craig J. Sturrock[1], Nils Stein[9,10], Martin Mascher[9,11], Roberto Tuberosa[3], Devin O'Connor[12], Malcolm J. Bennett[1,2], Anthony Bishopp[1], Silvio Salvi[3,*] and Rahul Bhosale[1,2,13,*]

***Corresponding authors**: Rahul Bhosale (rahul.bhosale@nottingham.ac.uk) and Silvio Salvi (silvio.salvi@unibo.it)

Article acceptance date: 29 March 2024

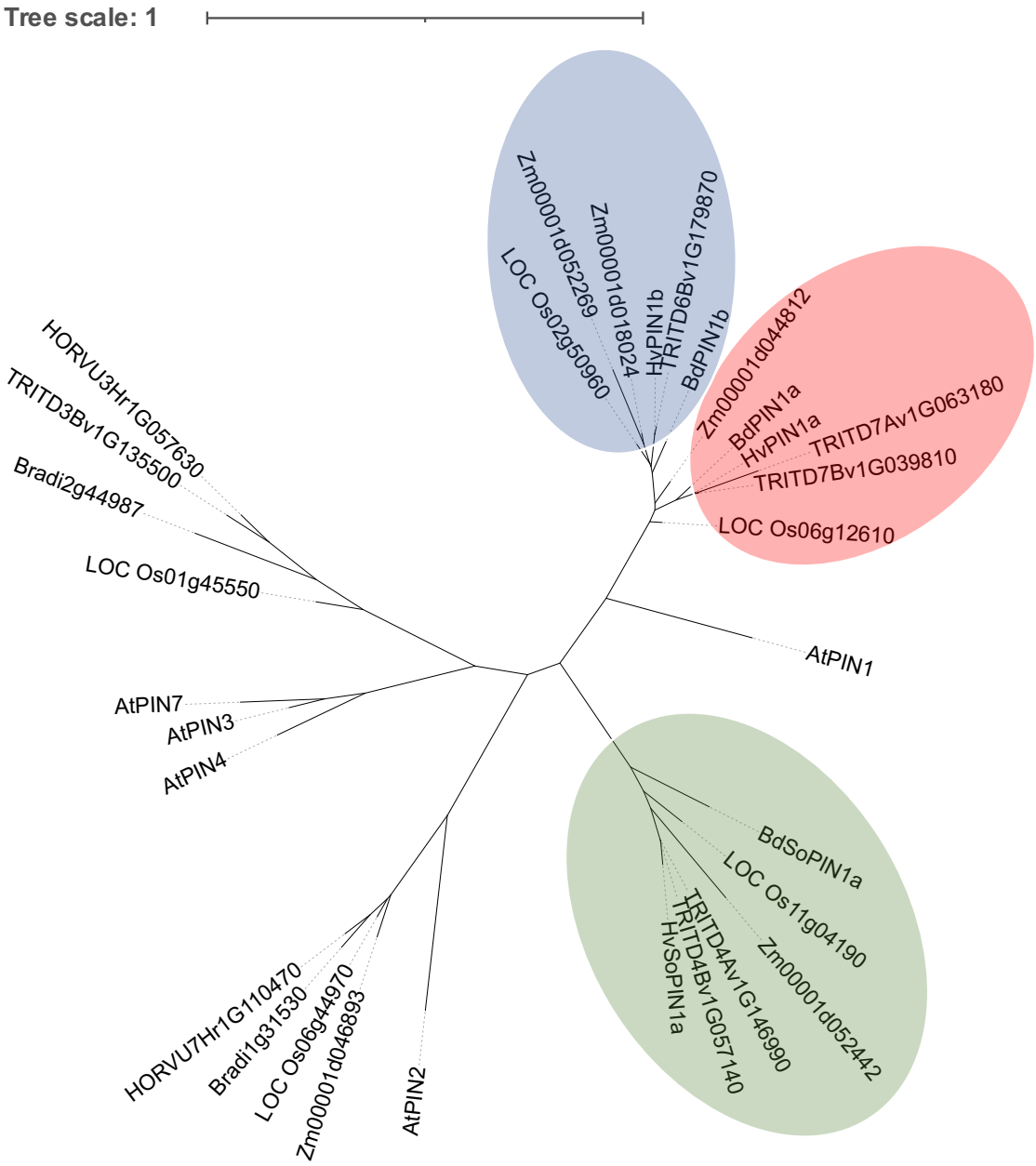

Fig. S1. Phylogenetic analysis of PIN Protein sequences in arabidopsis, barley, wheat, rice, maize and brachypodium.

AtPIN1 was used as a seed gene to select orthologous genes (>50% identity) from plant model arabidopsis (*Arabidopsis thaliana*) and key monocot species such as barley (*Hordeum Vulgare*), wheat (*Triticum ssp.*), rice (*Oryza sativa spp. japonica*), maize (*Zea mays B73*) and brachypodium (*Brachypodium distachyon*) using interactive phylogenetic module of Monocots Plaza 4.5 (Van Bel *et al.*, 2017). Protein sequences were aligned using MUSCLE (Edgar, 2004) and tree was constructed using FastTree (Price *et al.*, 2009) algorithm. Generated Newick file was imported into iTOL (Letunic & Bork, 2021) to create an unrooted tree. Red, blue and green color highlights the distinct clade formed by *Pin1a*, *Pin1b* and *SoPIN1a* members orthologous to *AtPIN1*.

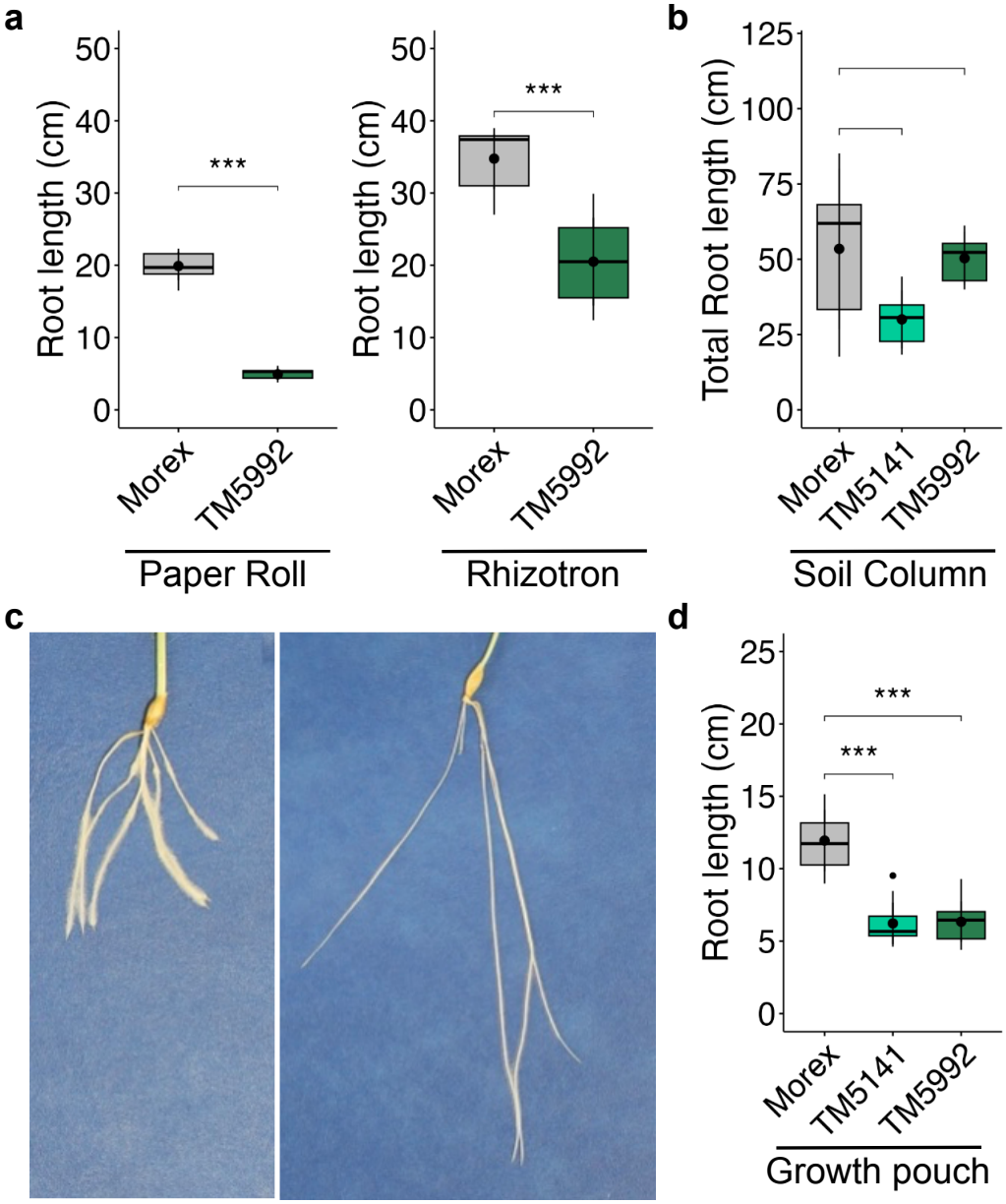

Fig. S2. Measured root growth parameters of *TM5992* and Morex.

a-b, Box plots showing average root length of Morex and *TM5992* grown in (**a**) paper roll and rhizotron for 9 days and (**b**) soil columns for 10 days. **c**, Representative image showing root architecture of Morex and *TM5992* grown in growth pouch system for 7 days. Scale bar = 2cm. **d**, Box plot showing average root length measured for (**c**). For all experiments, mean and standard deviations from 3 biological replicates, > 7 seedlings per replicate. *** indicates significance (*P*-value < 0.001, T-test).

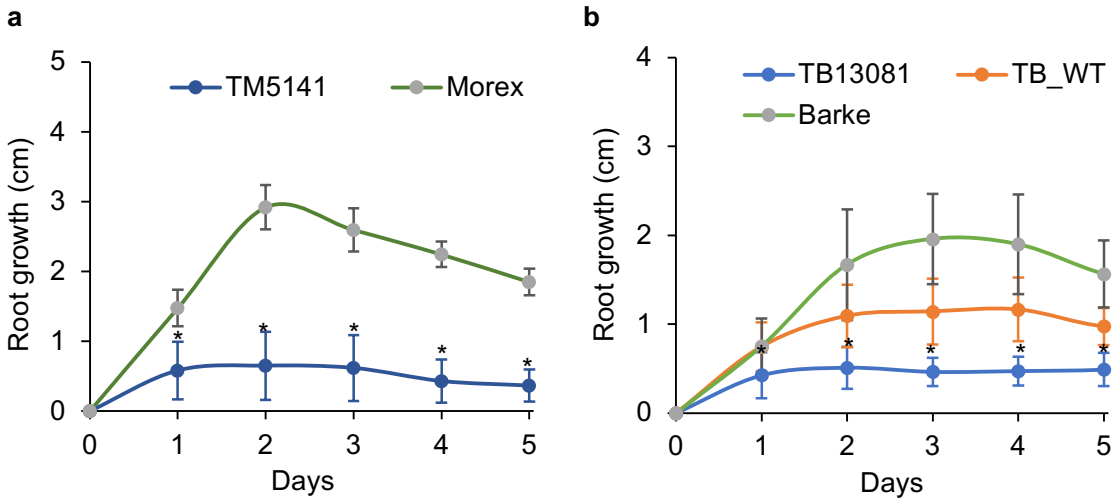

Fig. S3. *HvPIN1a* allelic mutant lines *TM5141* and *TB13081* exhibit similar root growth rate as line *TM5992*.

a, Line graph showing root growth rate of Morex and *TM5141* (second *Hvpin1a* mutant allele from Morex TILLING population). **b,** Line graph showing root growth rate of Barke, TB_WT (Barke TILLING background with functional *HvPIN1a*) and *TB13081* (third *Hvpin1a* mutant allele from Barke TILLING population) over 5 days post germination on 1% Agar plates. Both plots showing mean and standard deviations from at-least 2 biological replicates and included minimum 7 seedlings per replicate. * indicates significance (P-value < 0.01, *T-test*) between respective timepoints of Morex vs *TM5141* and Barke vs *TB13081*. TB_WT shows intermediate root growth rate between Barke and the mutant line TB13081. We suspect that the additional mutations carried in the TB_WT might have contributed to the observed root growth phenotype.

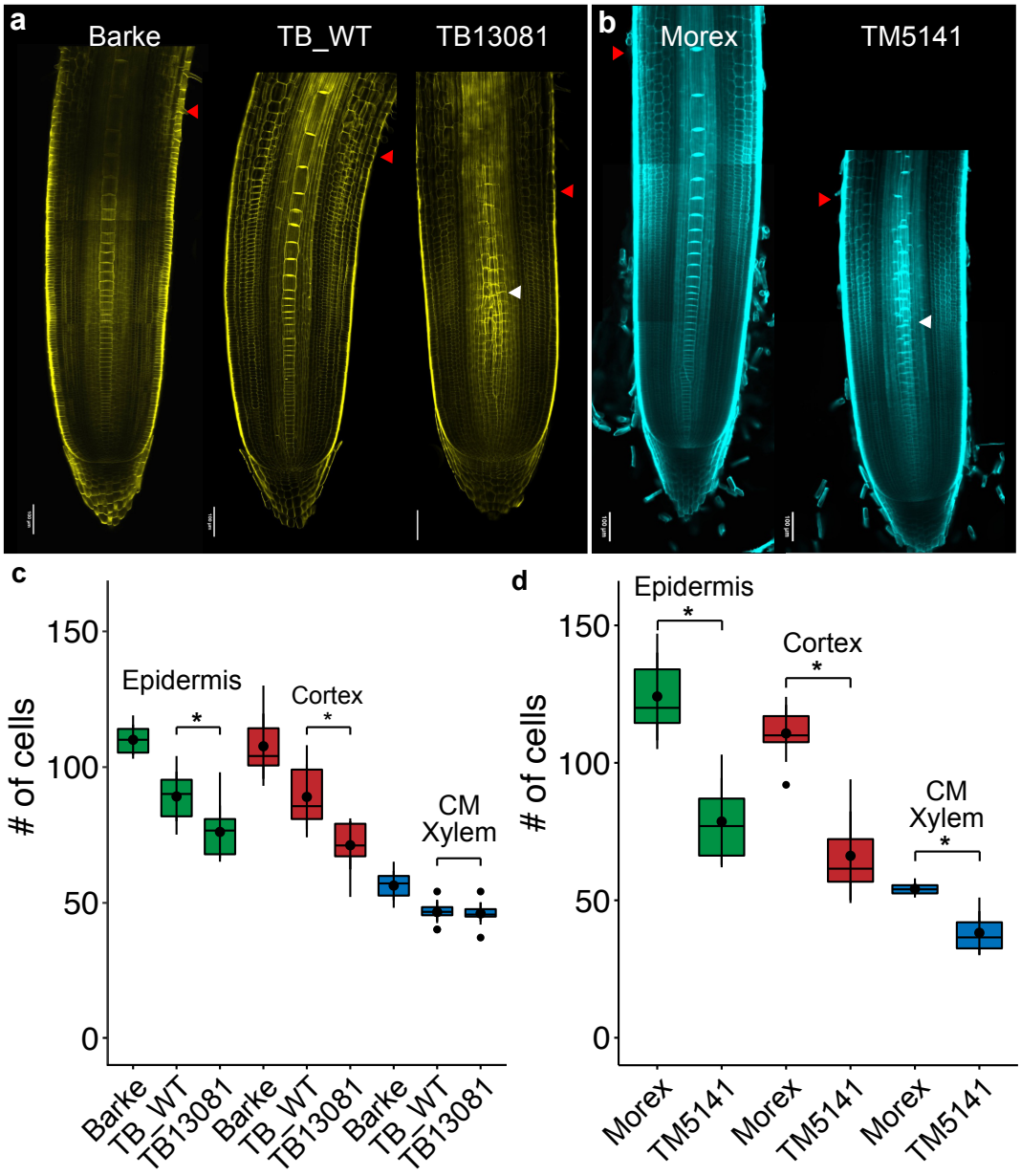

Fig. S4. *HvPIN1a* allelic mutant lines *TM5141* and *TB13081* exhibit similar root developmental defects as line *TM5992*.

a-b, Representative confocal image of longitudinal sections of (**a**) Barke, TB_WT and *TB13081* root tips stained with yellow direct 96 and (**b**) Morex and *TM5992* root tips stained with Calcofluor showing difference in first visible root hair (red) and visible defects in vascular patterning (white). Seedlings were vertically grown for 7 days on 1% Agar plates. N > 2 independent biological replicates and n > 5 seedlings per replicate were analysed. Scale bar = 100µm. **c-d**, Box plots showing distribution of number of cells in root epidermis, cortex and xylem tissues between quiescent center and first visible root hair in *TB13081* compared to Barke and TB_WT (**c**) and *TM5141* compared to Morex (**d**). Measurements were obtained from a clearly visible one cell file per tissue type. >8 seedlings were used for each genotype.

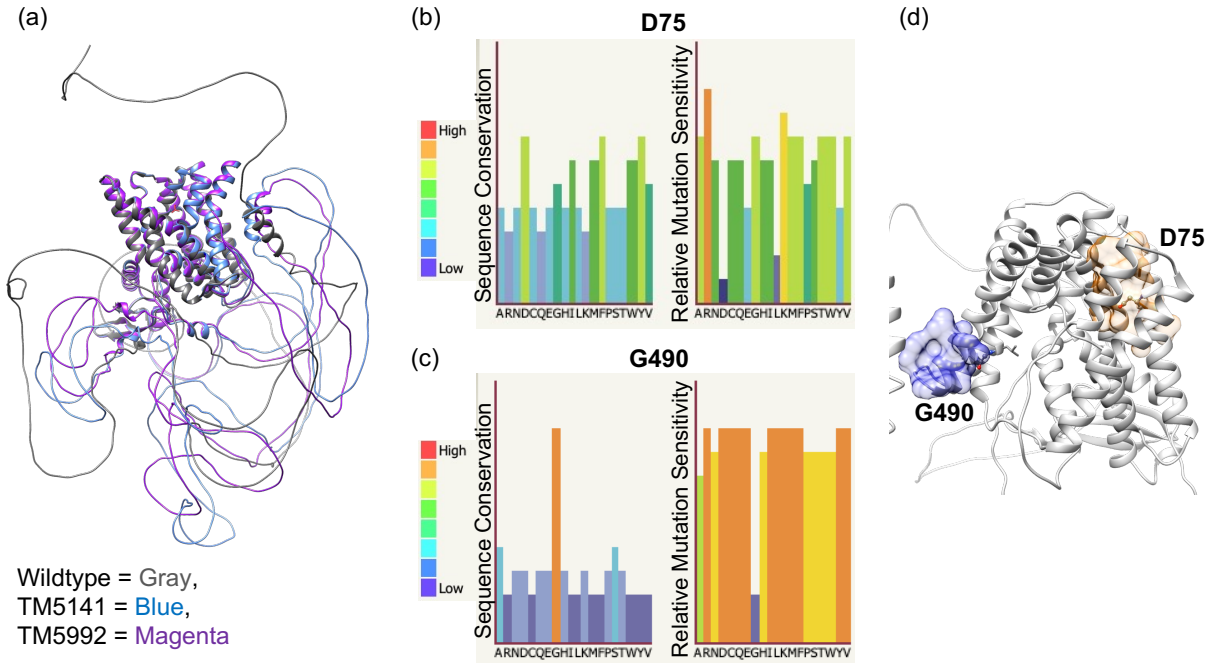

Fig. S5. Structure prediction of HvPIN1a and mutation mapping.

a, The structure of the N-terminal region (residues 10 – 110), which contains the *TM5141* (D75N) mutation, and the region between residues 450 – 550, which contains the *TM5992* (G490E) mutation, are predicted with high confidence (Jumper *et al.*, 2021; Mirdita *et al.*, 2022) and displayed remarkable similarity (RMSD = 0.596 Å) between the mutant and wildtype structures. The protein sequences outside these regions are more disordered and do not align well. **b-c**, Sequence conservation analysis using Jensen-Shannon Divergence (Kelley *et al.*, 2015) and mutation sensitivity predictions (Yates *et al.*, 2014) indicate that (**b**) position 75 has a moderate sequence preference for Asp, but lower sensitivity to a mutation to Asn, whereas (**c**) position 490 has a strong preference for Gly, and an equally high sensitivity to being mutated to Glu. **d,** Furthermore, binding site prediction on the HvPIN1a structure suggests the presence of two high ranking binding pockets close to these mutation sites. These pockets are depicted as blue surface near G490 and yellow surface near D75. G490 and D75 residues are represented as ball and stick models, while the rest of the protein structure is shown in ribbon representation. Computational docking (Flachsenberg *et al.*, 2024) of auxin within these pockets resulted in a higher docking score for the G490 pocket compared to the D75 pocket, indicating that auxin is more likely to bind the G490 pocket. Overall, the sequence conservation, mutation sensitivity and docking site analysis comprehensively suggest that the G490E mutation would introduce large negative residue at a sensitive region on the HvPIN1a structure, which will also likely negatively affect the binding function of the protein in this region. By way of comparison, the effect of D75N mutation is predicted to have milder effects on the structural stability and binding function of the protein.

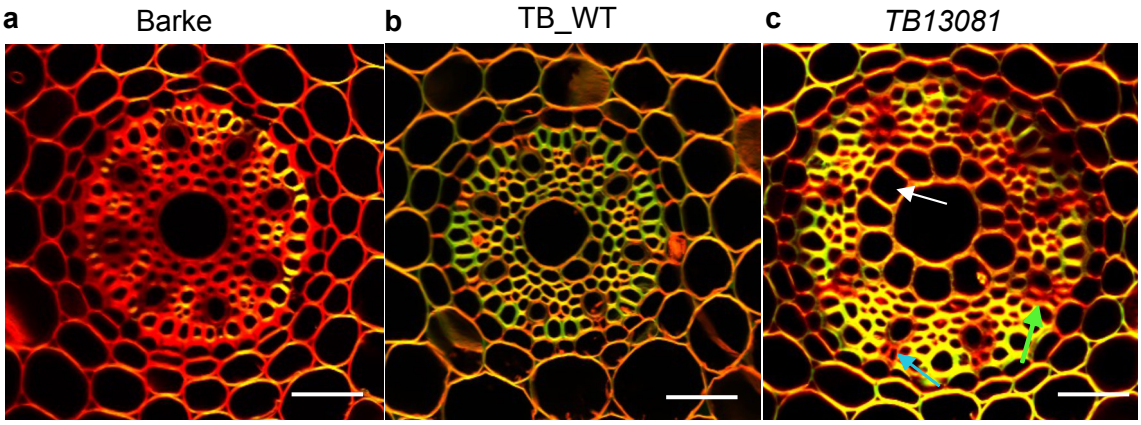

Fig. S6. *HvPIN1a* allelic mutant line *TB13081* exhibit similar root anatomical defects as lines *TM5992* and *TM5141*.

a-c, Representative confocal images root cross-sections of Barke (**a**), TB_WT (**b**) and *TB13081* (**c**). Seedlings were vertically grown for 7 days on 1% Agar, and mid regions (~3-4 cm from the root apex) of the seminal roots were cross-sectioned and imaged using confocal (Red = PI stain and Green = autofluorescence). Blue, green and white arrows in (**c**) indicate irregularities in protoxylem, peripheral metaxylem vessels and first parenchymatic cell layer around the central metaxylem. *N* > 3 independent biological replicates and *n* > 5 seedlings per replicate. Scale bar = 50µm.

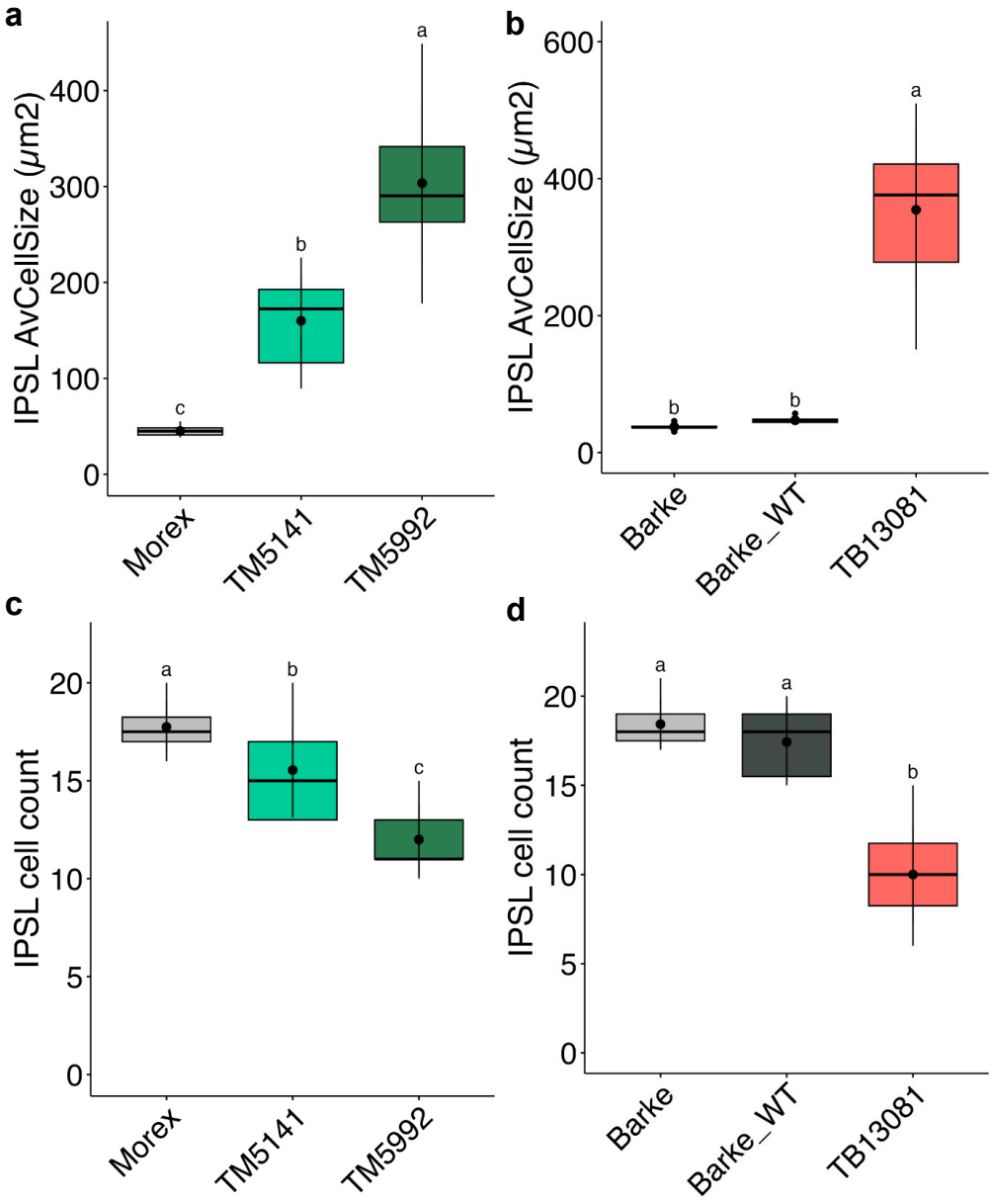

Fig. S7. *HvPIN1a* allelic mutants show enlarged parenchymatic cells in the inner stele layer surrounding central metaxylem.

a-d, Box plots showing data quantification of root cross section images showing differences in the Inner Parenchymatic Stele Layer surrounding central metaxylem (IPSL) cell sizes (**a-b**) and cell numbers (**c-d**) of *Hvpin1a* mutant alleles (*TM5141*, *TM5992* and *TB13081*) compared to their respective wildtypes (Morex and Barke and TB_WT). Significant differences were determined using Anova and Tukey's test with an alpha level of 0.05, denoted by different letters.

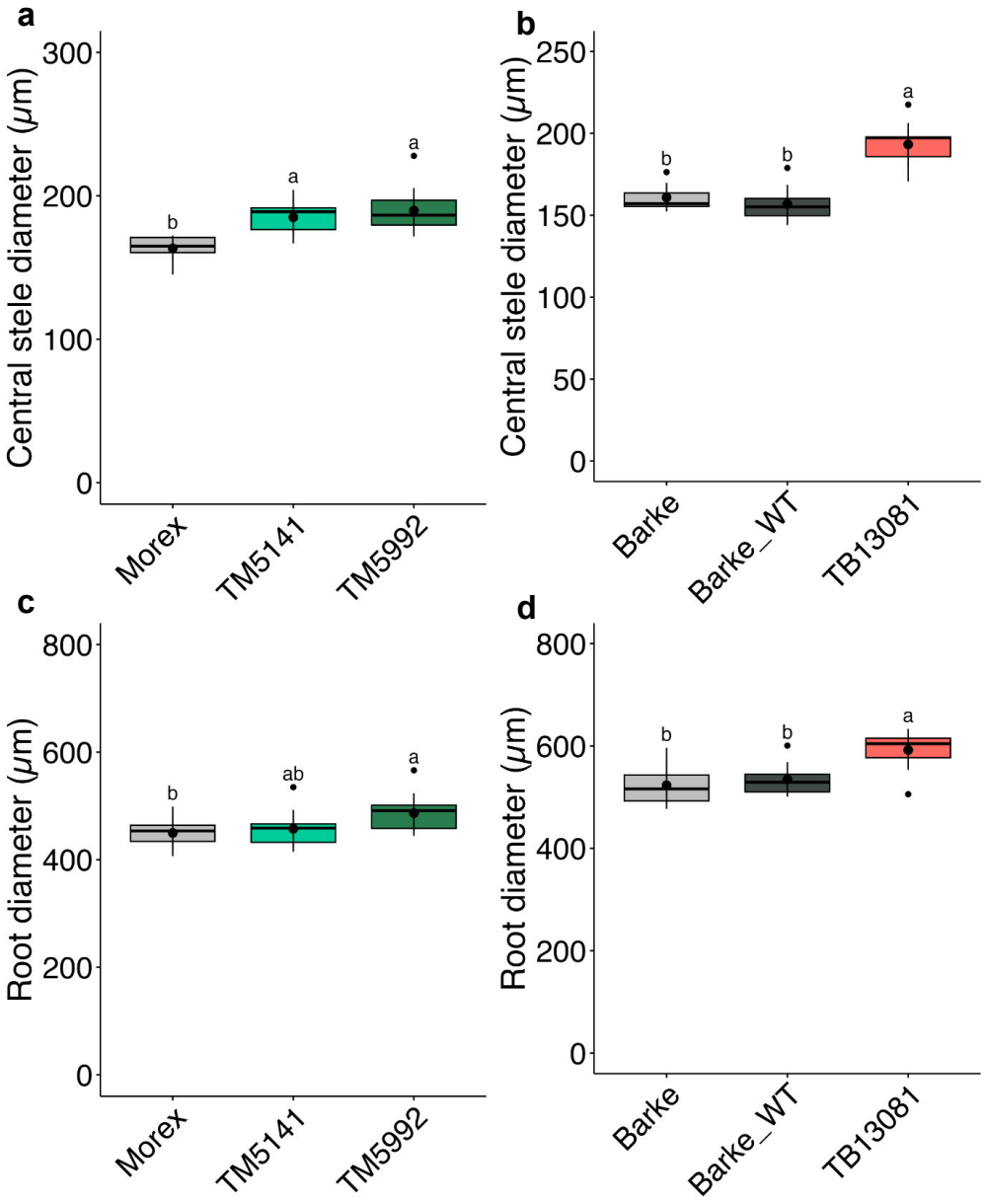

Fig. S8. *HvPIN1a* allelic mutants show an enlarged stele and root diameter.

a-d, Box plots showing data quantification of root cross section images showing differences in the stele (**a-b**) and root (**c-d**) diameter of *Hvpin1a* mutant alleles (*TM5141*, *TM5992* and *TB13081*) compared to their respective wildtypes (Morex and Barke and TB_WT). Significant differences were determined using Anova and Tukey's test with an alpha level of 0.05, denoted by different letters.

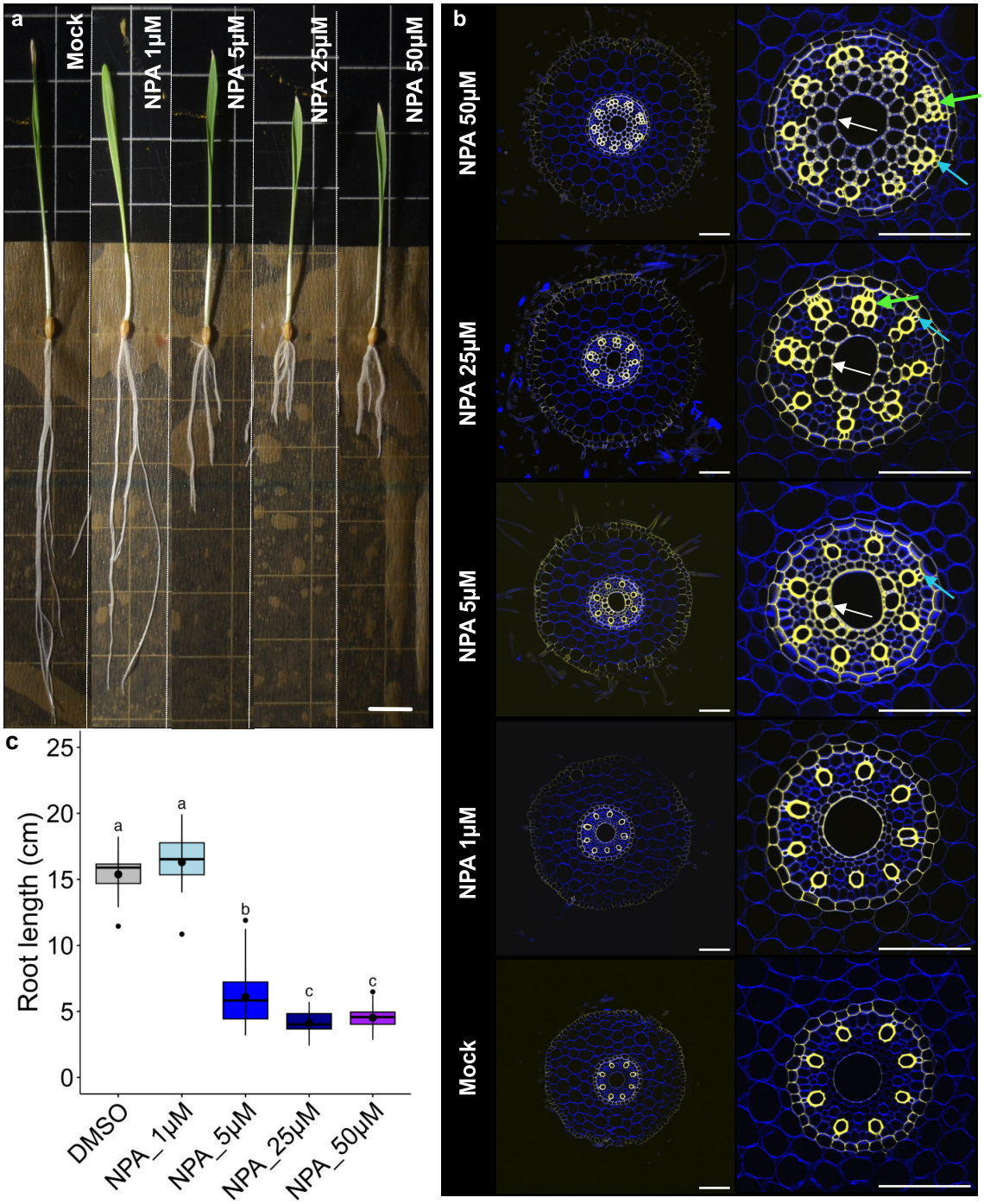

Fig. S9. NPA treatment induces short root phenotype and vascular patterning defects in the wild-type Morex roots similar to those observed in *HvPIN1a* mutant alleles.

a, Representative images showing the root growth of 5 days old Morex seedlings grown on 1% Agar supplemented with DMSO (Mock) and treated with increasing concentration of NPA (1,5,25,50 µM) dissolved in DMSO. Scale bar = 2 cm. **b**, Representative confocal images showing whole root cross sections (left) and magnified stele regions (right), stained with Calcofluor White (Blue) and Basic Fuschin (Yellow) to mark cell walls and lignin deposition. Scale bar = 100 µm. Blue, green and white arrows indicate irregularities in protoxylem, peripheral metaxylem vessels and inner parenchymatic cell layer around the central metaxylem. **c**, Box plot showing root length quantification for (a). Images were collected from n = > 6 individual seedlings per replicate per treatment, 3 biological replicates, and processed using ImageJ. Scale bar=100µm. Different letters indicate statistically significant differences for *alpha* = 0.05 using ANOVA and Tuckey test in R.

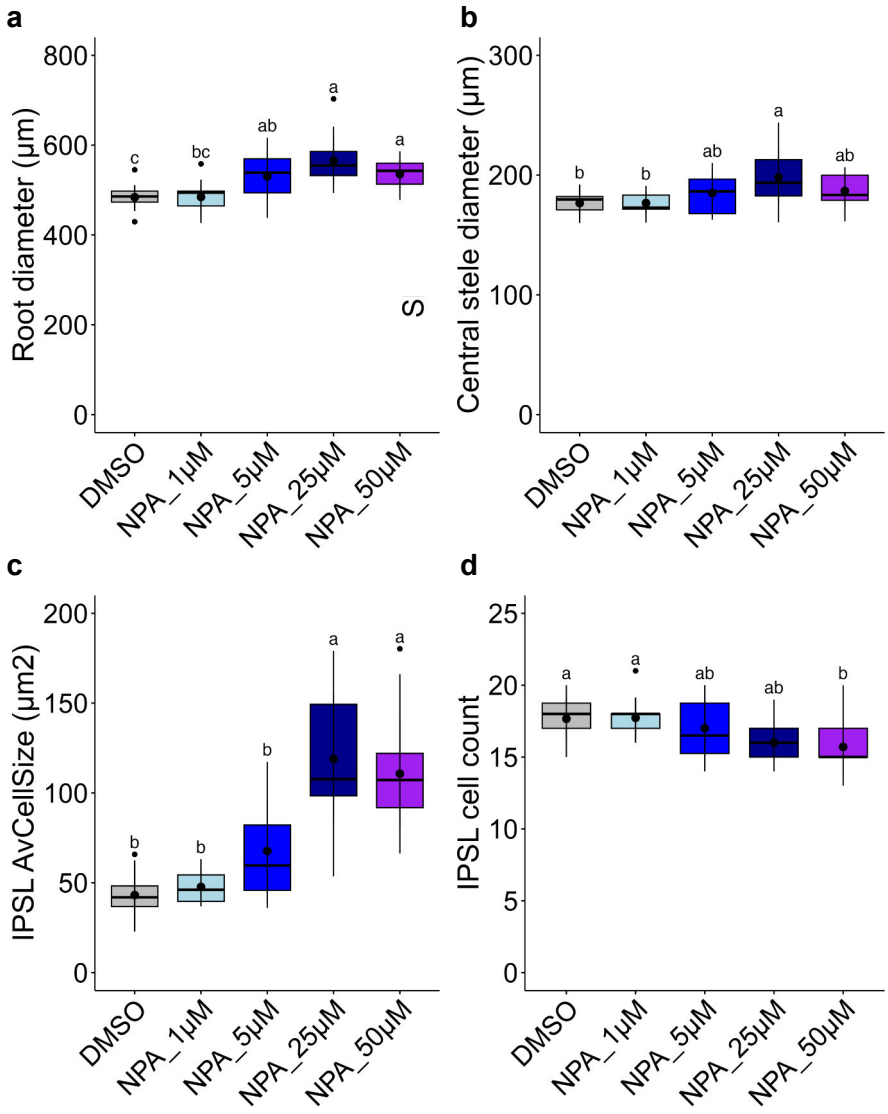

Fig. S10. NPA treatment increases root and stele diameter in wildtype Morex similar to those observed in *HvPIN1a* mutant alleles.

a-d, Box plots showing data quantification showing root (**a**) and stele diameter (**b**) and IPSL average cell size (**c**) and cell count (**d**) of Morex roots grown in paper rolls supplemented with DMSO (control) and increasing concentration of NPA (1, 5, 25, 50 µM). Images were collected from n = > 6 individual seedlings per replicate per treatment, 3 biological replicates, and processed using ImageJ. Scale bar=100µm. Different letters indicate statistically significant differences for *alpha* = 0.05 using ANOVA and Tuckey test in R.

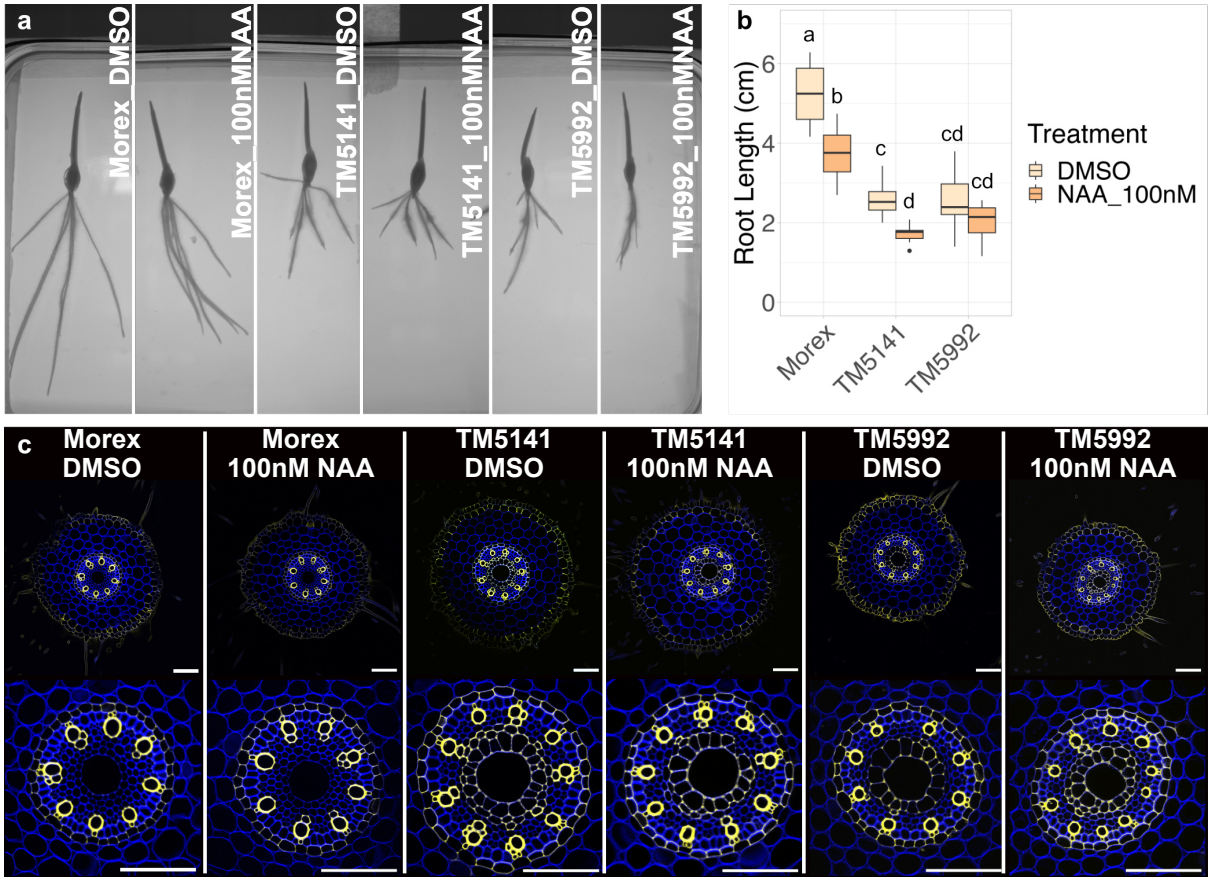

Fig. S11. NAA treatment does not rescue wild-type phenotypes in *HvPIN1a* mutant alleles.

a, Representative images showing the effect of 100nM NAA treatment compared to mock DMSO on root lengths of wildtype Morex and *Hvpin1a* mutant alleles *TM5992* and *TM5141*. **b,** Box plot showing root length quantification for (**a**). Significant differences were determined using Anova and Tukey's test with an alpha level of 0.05, denoted by different letters. Images were collected from n = > 5 individual seedlings per treatment and processed using ImageJ. **c**, Representative confocal images showing whole root cross sections (top) and magnified stele regions (bottom), stained with Calcofluor White (Blue) and Basic Fuchsin (Yellow) to mark cell walls and lignin deposition. Scale bar = 100µm.

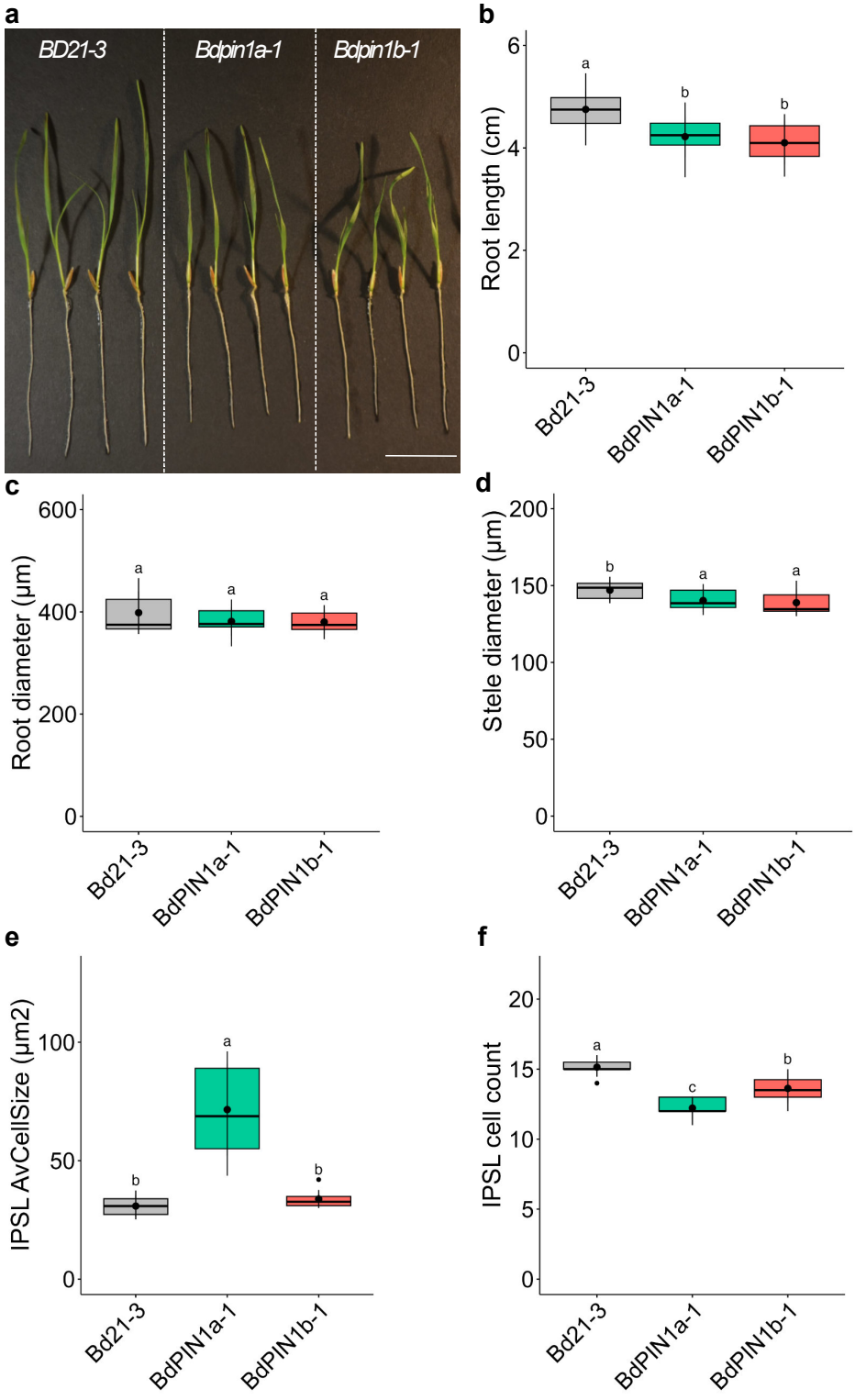

Fig. S12. Root growth and anatomy comparison between Brachypodium wildtype (Bd21.3) and *Bdpin1* mutants (*Bdpin1a*, *Bdpin1b*).

a-b, Representative image (**a**) and root length data quantification (**b**) of 7day old seedlings of wildtype Bd21.3 and *Bdpin1a* mutant grown in ½ MS media, *n* = >13 independent seedlings. **c-e**, Box plots showing data quantification showing differences in the root (**c**) and stele (**d**) diameter and the IPSL average cell sizes (**e**) and cell numbers (**f**) of *Bdpin1a and Bdpin1b* mutants (O'Connor *et al.*, 2014, 2017) compared to wildtype Bd21-3. Different letters indicate statistically significant differences for *alpha* = 0.05 using ANOVA and Tuckey test in R.

SI datasets

Dataset S1. Exome sequencing and mapping of *TM5992* reads to Morex reference identified 16 mutations within genes on Chromosome 7H. Red highlighted rows indicate three mutations within region of interest identified by Bulk Segregant Analysis.

SI References

1. **Edgar RC**. **2004**. MUSCLE: multiple sequence alignment with high accuracy and high throughput. *Nucleic Acids Research* **32**: 1792–1797.
2. **Flachsenberg F, Ehrt C, Gutermuth T, Rarey M**. **2024**. Redocking the PDB. *Journal of Chemical Information and Modeling* **64**: 219–237.
3. **Jumper J, Evans R, Pritzel A, Green T, Figurnov M, Ronneberger O, Tunyasuvunakool K, Bates R, Žídek A, Potapenko A, *et al.* 2021**. Highly accurate protein structure prediction with AlphaFold. *Nature* **596**: 583–589.
4. **Kelley LA, Mezulis S, Yates CM, Wass MN, Sternberg MJE**. **2015**. The Phyre2 web portal for protein modeling, prediction and analysis. *Nature Protocols* **10**: 845–858.
5. **Letunic I, Bork P**. **2021**. Interactive Tree Of Life (iTOL) v5: an online tool for phylogenetic tree display and annotation. *Nucleic Acids Research*: gkab301–.
6. **Mirdita M, Schütze K, Moriwaki Y, Heo L, Ovchinnikov S, Steinegger M**. **2022**. ColabFold: making protein folding accessible to all. *Nature Methods* **19**: 679–682.
7. **O'Connor DL, Elton S, Ticchiarelli F, Hsia MM, Vogel JP, Leyser O**. **2017**. Cross-species functional diversity within the PIN auxin efflux protein family. *eLife* **6**: e31804.
8. **O'Connor DL, Runions A, Sluis A, Bragg J, Vogel JP, Prusinkiewicz P, Hake S**. **2014**. A Division in PIN-Mediated Auxin Patterning during Organ Initiation in Grasses. *PLoS Computational Biology* **10**: e1003447.
9. **Price MN, Dehal PS, Arkin AP**. **2009**. FastTree: Computing Large Minimum Evolution Trees with Profiles instead of a Distance Matrix. *Molecular Biology and Evolution* **26**: 1641–1650.
10. **Van Bel M, Diels T, Vancaester E, Kreft L, Botzki A, Van de Peer Y, Coppens F, Vandepoele K**. **2017**. PLAZA 4.0: an integrative resource for functional, evolutionary and comparative plant genomics. *Nucleic Acids Research* **46**: gkx1002–.
11. **Yates CM, Filippis I, Kelley LA, Sternberg MJE**. **2014**. SuSPect: Enhanced Prediction of Single Amino Acid Variant (SAV) Phenotype Using Network Features. *Journal of Molecular Biology* **426**: 2692–2701.